ChemComm

COMMUNICATION

View Article Online
View Journal | View Issue

Cite this: *Chem. Commun.*, 2014, **50**, 8398

Received 2nd April 2014,
Accepted 13th June 2014

DOI: 10.1039/c4cc02412e

www.rsc.org/chemcomm

Poly β-cyclodextrin inclusion-induced formation of two-photon fluorescent nanomicelles for biomedical imaging†

Huijuan Yan,[a] Leiliang He,[a] Cheng Ma,[a] Jishan Li,*[a] Jinfeng Yang,[b] Ronghua Yang*[a] and Weihong Tan[a]

A novel two-photon absorption (TPA) nanomicelle through the "host-guest" chemistry has been developed and successfully applied in tumor tissue imaging in this work.

Two-photon excitation (TPE) with near infrared (NIR) photons as the excitation source has the advantages of lower tissue autofluorescence and self-absorption, reduced photodamage and photobleaching, high spatial resolution and deeper penetration depth (>500 μm), *etc.* Together with the development of two-photon microscopy (TPM), TPE has become a powerful tool for research in life science and TP bioimaging applications.[1] The quality of two-photon fluorescence imaging in biological media is highly dependent on the two-photon absorption (TPA) materials, which should have large two-photon action cross-sections, good solubility and biocompatibility.[2] Recently, although a variety of TPA organic molecules[3] and TPA inorganic nanomaterials (*e.g.* metal clusters,[4] semiconductor quantum dots[5] and carbon nanomaterials[6]) have been developed and successfully applied in the fields of biomedical imaging and biosensing, the low fluorescence quantum yield and slow delivery across membranes for organic molecules, possible cytotoxicity and the need for further hydrophilic and complex functional modification processes for inorganic nanomaterials are still the limitations for their wide range of applications in biomedical imaging. Therefore, the search for new TPA materials with excellent characteristics such as good biocompatibility, high cell permeability and high TPA action cross-section, has become increasingly important and urgent.

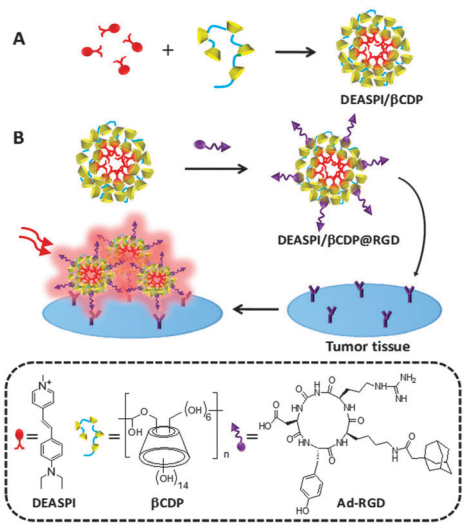

Scheme 1 Schematic illustration of fabrication of the DEASPI/βCDP nanomicelles (A) and application in TPE tumor tissue imaging (B).

Herein, as shown in Scheme 1, we constructed a β-cyclodextrin polymer (βCDP)-based TPA fluorescent nanomicelle *via* the inclusion interaction between β-cyclodextrin (βCD) and *trans*-4-[*p*-(*N*,*N*-diethylamino)styryl]-*N*-methylpyridinium iodide (DEASPI) (for the synthesis of βCDP and DEASPI, see ESI†), and the further functionalized TPA fluorescent nanomicelles were applied in biomedical imaging. βCD as a member of the cyclodextrin (CD) family is a widely used host molecule capable of internalizing guest molecules in water with binding constants in the $10^{0.5}$–10^{5} M^{-1} range.[7] βCD and its assemblies have been extensively used in biomedical fields ranging from drug solubilization to their use as a building block for nonviral vector construction because of their high solubilization ability, low toxicity and their ability to destabilize and permeate biological membranes and for obviating undesirable side effects.[8] In our research, we found that a small TPA organic molecule can be encased into the cavity of βCD to form the βCDP-based nanomicelle and the TP action cross-section of the small TPA organic molecule can be

[a] *State Key Laboratory of Chemo/Biosensing and Chemometrics, College of Chemistry and Chemical Engineering, Hunan University, Changsha 410082, China. E-mail: jishanli@hnu.edu.cn, yangrh@pku.edu.cn; Fax: +86 731 88822587; Tel: +86 731 88822587*

[b] *Tumor Hospital of Xiangya School of Medicine, Central South University, Changsha 410013, China*

† Electronic supplementary information (ESI) available: Experimental details, synthesis and characterization of DEASPI and βCDP, one-photon luminescence spectra and the photostability test, MTT assay and targeted cell two-photon imaging. See DOI: 10.1039/c4cc02412e

enhanced greatly. These findings have led us to explore the design and construction of a new TPA supramolecular architecture based on the "host–guest" chemistry for application in biomedical imaging, which has not been reported to the best of our knowledge.

The morphology and structure of the DEASPI/βCDP nanomicelle were first investigated by using dynamic light-scattering (DLS), TEM imaging and circular dichroism spectra. DLS showed that the complex size produced by DEASPI and βCDP was about 100 nm, while the size of βCDP was only about 5.0 nm (Fig. S1, ESI†). To confirm formation of the DEASPI–βCD complex *via* host–guest interaction, its circular dichroism spectra were measured (Fig. S2, ESI†). All the solutions of DEASPI, βCD and βCDP showed no significant circular dichroism spectra band, while a mixture of βCDP and DEASPI showed a strong positive Cotton band at around 470 nm, which was similar to that of the βCD–DEASPI mixture. This phenomenon can be explained by the observation that the achiral compounds located in the CD cavity will produce induced circular dichroism signals in the corresponding transition bands, and the sign of circular dichroism is positive for a transition polarized parallel to the axis of the macrocyclic host.[9] Both DLS and circular dichroism spectra of the samples indicate that the nanoscaled supramolecular polymer complex can be formed in the presence of the guest molecule DEASPI. Relative to the DLS results, TEM images showed that the morphology of βCDP is irregular film-shaped objects (Fig. 1a) while the DEASPI–βCDP complexes exhibit spherical geometry with the average diameters of ~60 nm (Fig. 1b). The sizes determined by TEM are smaller than those measured by DLS due to the relative dry nature of the TEM samples. In order to further demonstrate that the formation of nanomicelles resulted from the inducement of host–guest interaction between DEASPI and βCD rather than the encapsulation of DEASPI into the cavums of βCDP-based particles, the βCDP was first incubated with adamantine and then DEASPI was added. DLS showed that the size of this product is about 5.0 nm similar to that of βCDP, and the TEM image showed that its morphology is also of irregular film shape (Fig. S3, ESI†), which indicates that the DEASPI/βCDP-based nanomicelles were not formed due to the formation of a more stable inclusion complex between βCD and adamantine, demonstrating that the host–guest inclusion interaction between DEASPI and βCD is the primary factor for the formation of nanomicelles.

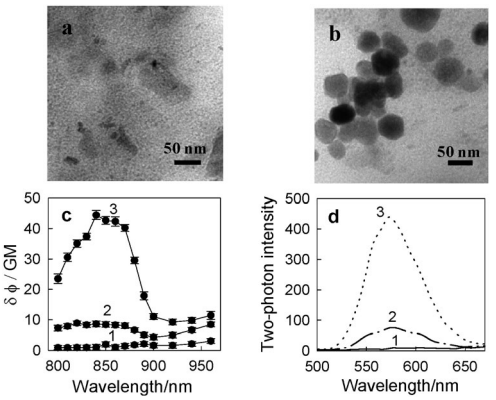

Fig. 1 TEM images of βCDP (a) and DEASPI/βCDP nanomicelles (b). TPE action cross sections (c) and TPE fluorescence emission spectra (d) of the aqueous solutions. 1: 10 μM of DEASPI; 2: 10 μM of DEASPI + 0.5 mg mL^{-1} of βCD; 3: 10 μM of DEASPI + 0.5 mg mL^{-1} of βCDP. For 'c', λ_{ex} = 800–960 nm; for 'd', λ_{ex} = 840 nm.

The TPA action cross section ($\delta\Phi$, the product of the TPA cross-section (δ) and the fluorescence quantum yield (Φ)) and the TPE emission spectra of the DEASPI/βCDP nanomicelles were then measured carefully. As shown in Fig. 1c, the maximal $\delta\Phi$ of the DEASPI molecule in the DEASPI/βCDP nanomicelles was measured to be 44.5 GM (λ_{ex} = 840 nm, 1 GM = 10^{-50} cm^4 s $photon^{-1}$ $molecule^{-1}$) with rhodamine 6G as the reference,[10] which was much higher than that of the DEASPI molecule (1.0 GM) or the DEASPI/βCD inclusion complex (8.6 GM). The TPE emission spectra of the DEASPI/βCDP nanomicelles are shown in Fig. 1d. One can see that the TPE fluorescence emission intensity of this nanomicelle can be enhanced up to *ca.* 40 times compared to that when DEASPI is directly dissolved in aqueous solution, while only about 5-times enhancement is observed when a βCD monomer was used. These TPE fluorescence emission spectra are similar to those obtained in one-photon excitation (OPE) experiments (Fig. S4, ESI†); very weak one photon-induced emission was also observed for either DEASPI or DEASPI/βCD owing to their lower fluorescence quantum yield (the Φ is 0.47, 0.02 and 0.10 for DEASPI/βCDP, DEASPI or DEASPI/βCD inclusion complex, respectively (Table S1, ESI†)), indicating that the formation of nanomicelles can offer a more protective micro-environment to decrease the effect of the twisted intra-molecular charge transfer (TICT) process on the embedded DEASPI.

Stability of the prepared nanomicelles under various environmental conditions, for example, different pH values, different ion concentrations (Na^+, K^+, Ca^{2+}, Mg^{2+}), human serum or human cell lysate-contained biological fluids and irradiation by using a 150 W xenon lamp as the excitation source, was first investigated through testing its fluorescence intensity (Fig. S5, ESI†). The results show that the prepared fluorescent nanomicelles have good photostability, are stable at around the physiological pH value, have high ion strength, biological conditions and a long storage time. Furthermore, cellular cytotoxicity assay of the DEASPI/βCDP nanomicelles towards HeLa and MCF-7 cells as the model shows that no apparent cytotoxicity was observed for these two cells even when the concentration of this nanomicelle was increased up to 2.5 mg mL^{-1} (~50 μM DEASPI) (Fig. S6, ESI†). The cytotoxicity of this nanomicelle is much lower than that of the DEASPI molecules alone which killed 32% HeLa cells and 22% MCF-7 cells, respectively, at a similar concentration of materials. The high biocompatibility of βCDP and the efficient shielding of organic molecules by the matrix in the βCDP-based nanomicelles may be a cause of the low cytotoxicity of this TPA nanomicelle to cells.

To demonstrate the practical applications of this prepared TPA nanomicelle in biomedical imaging or clinical diagnostics, a cyclic RGD peptide (c(RGDyK)) conjugated adamantine (denoted as Ad-RGD) was anchored on the surface of the βCDP-based nanomicelle to form a TPA bionanoprobe (DEASPI/βCDP@RGD) by the βCD/adamantine host–guest inclusion strategy (Scheme 1B, Fig. S7 in ESI†). The c(RGDyK) selectively recognizes $\alpha_v\beta_3$ and $\alpha_v\beta_5$ integrin receptors, which plays a pivotal role in angiogenesis,

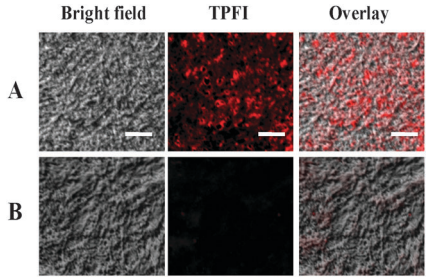

Fig. 2 TPE fluorescence images of frozen cervical cancer tumor tissue slice (A) and frozen normal cervical tissue slice (B) stained with DEASPI/βCDP@RGD. Scale bars: 40 μm.

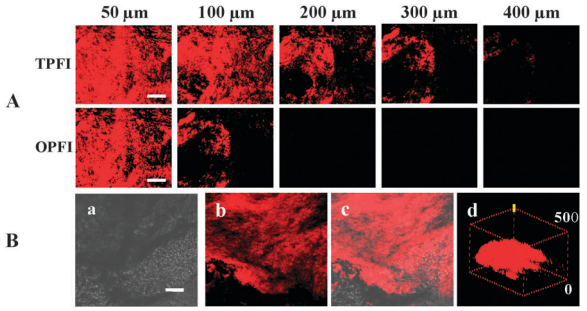

Fig. 3 Confocal fluorescence images of a part of a fresh thick cervical tumor tissue slice stained with DEASPI/βCDP@RGD. (A) *Z*-Scan TPE (TPFI) and OPE (OPFI) fluorescence images at different penetration depths, the scale bar is 80 μm; (B) bright-field image (a), TPE fluorescence image (b), overlay image (c) and the 3D reconstruction from 50 *Z*-scan TPE imaging sections at a depth of 0–500 μm with 60× magnification (d), the scale bar is 60 μm.

vascular intima thickening, and proliferation of malignant tumors.[11] HeLa cells possessing $\alpha_v\beta_3/\alpha_v\beta_5$ integrins and integrin-negative cells (MCF-7) were first chosen as model cell lines to investigate the targeting effect.[12] It can be seen clearly from Fig. S8 (ESI†) that DEASPI/βCDP@RGD did not bind to integrin-negative cells (MCF-7) after a 30 min-incubation time because a minimal fluorescence signal is observed, whereas the integrin-positive cells (HeLa) are clearly visualized and the staining can be blocked effectively by 10 μM c(RGDyK). Additionally, the non-RGD-conjugated DEASPI/βCDP nanomicelle had minimal nonspecific binding at the same incubation time of 30 min. These results demonstrate that the DEASPI/βCDP@RGD can selectively bind to integrin $\alpha_v\beta_3/\alpha_v\beta_5$-rich tumor cells. Next the DEASPI/βCDP@RGD was used for imaging diagnosis of cervical cancer. Fig. 2 shows the DEASPI/βCDP@RGD staining of frozen slices of the cervical tumor tissues and the normal cervical tissues, respectively. Strong fluorescence signals can be observed for the cervical tumor tissue slice, while the normal cervical tissue slice gave virtually no fluorescence signal. Moreover, no obvious fluorescence was noted for both the cervical tumor tissue slice and the normal cervical tissue slice stained with DEASPI/βCDP (Fig. S9, ESI†). The above confocal images clearly demonstrate the high $\alpha_v\beta_3/\alpha_v\beta_5$ integrin expression level of the cervical cancer.

To further demonstrate the deep imaging capacity of the prepared TPA nanomicelle, after incubation of a 2.0 mm-thick cervical tumor tissue slice with DEASPI/βCDP@RGD, the fluorescence imaging was performed by two-photon confocal microscopy. The *Z*-scanning confocal imaging shows that bright TPE fluorescence emission was still present until 300 μm of penetration depth, while no significant OPE fluorescence can be observed when the penetration depth was only more than 100 μm (Fig. 3A), indicating that the prepared TPA nanomicelles have the capacity of depth tissue imaging. Then the 3D reconstitution of confocal XYZ scanning micrographs is obtained from 50 confocal *Z*-scan TPE imaging sections ('d' of Fig. 3B), which indicates that the DEASPI/βCDP@RGD nanoprobes are evenly distributed in HeLa tissues and have a high signal-to-noise ratio.

In conclusion, a facile strategy for TPA fluorescent nanomicelle preparation has been developed through the "host–guest" chemistry. This βCDP-based TPA fluorescent nanomicelle exhibits desirable two-photon-sensitized fluorescence properties, high photostability, high cell-permeability, high stability and excellent biocompatibility. As a result, by anchoring the RGD peptide on the nanomicelle's surface *via* the high binding affinity of labeled adamantine with βCD, the targeted TPE imaging has been successfully achieved in cancer cells and tumor tissues. To the best of our knowledge, it is the first time that the βCDP-based two-photon fluorescent nanoprobe has been successfully used in cancer cells and tissues. The material design approach reported here also opens up new perspectives for developing a wide range of unique sensing schemes and will have great potential in cancer diagnosis and biomedical research, which are compatible with the benefits of multiphoton imaging techniques.

The authors would like to acknowledge the financial support from NSFC (21135001, 21205143 and J1103312), the Program for New Century Excellent Talents in University (NCET-13-0188) and the "973"National Key Basic Research Program (2011CB91100-0). The authors also thank Professor Zhihong Liu of Wuhan University for the TPE spectra measurements.

Notes and references

1 (*a*) F. Helmchen and W. Denk, *Nat. Methods*, 2005, **2**, 932–940; (*b*) D. A. Parthenopoulos and P. M. Rentzepis, *Science*, 1989, **245**, 843–845; (*c*) S. Kawata and Y. Kawata, *Chem. Rev.*, 2000, **100**, 1777–1788; (*d*) H. M. Kim and B. R. Cho, *Acc. Chem. Res.*, 2009, **42**, 863–872; (*e*) H. J. Kim, C. H. Heo and H. M. Kim, *J. Am. Chem. Soc.*, 2013, **135**, 17969–17977; (*f*) S. K. Bae, C. H. Heo, D. J. Choi, D. Sen, E.-H. Joe, B. R. Cho and H. M. Kim, *J. Am. Chem. Soc.*, 2013, **135**, 9915–9923.

2 (*a*) S. Kim, Q. D. Zheng, G. S. He, D. J. Bharali, H. E. Pudavar, A. Baev and P. N. Prasad, *Adv. Funct. Mater.*, 2006, **16**, 2317–2323; (*b*) K. Li, Y. H. Jiang, D. Ding, X. H. Zhang, Y. T. Liu, J. L. Hua, S. S. Feng and B. Liu, *Chem. Commun.*, 2011, **47**, 7323–7325.

3 (*a*) G. S. He, L. S. Tan, Q. D. Zheng and P. N. Prasad, *Chem. Rev.*, 2008, **108**, 1245–1330; (*b*) S. Sumalekshmy and C. J. Fahrni, *Chem. Mater.*, 2011, **23**, 483–500; (*c*) S. Yao and K. D. Belfield, *Eur. J. Org. Chem.*, 2012, 3199–3217.

4 (*a*) G. Ramakrishna, O. Varnavski, J. Kim, D. Lee and T. Goodson, *J. Am. Chem. Soc.*, 2008, **130**, 5032–5033; (*b*) S. A. Patel, C. I. Richards, J. C. Hsiang and R. M. Dickson, *J. Am. Chem. Soc.*, 2008, **130**, 11602–11603.

5 (*a*) J. Z. Wang, M. Lin, Y. L. Yan, Z. Wang, P. C. Ho and K. P. Loh, *J. Am. Chem. Soc.*, 2009, **131**, 11300–11301; (*b*) L. Jauffred and L. B. Oddershede, *Nano Lett.*, 2010, **10**, 1927–1930; (*c*) E. J. McLaurin, A. B. Greytak, M. G. Bawendi and D. G. Nocera, *J. Am. Chem. Soc.*, 2009, **131**, 12994–13001.

6 (*a*) J. L. Li, H. C. Bao, X. L. Hou, L. Sun, X. G. Wang and M. Gu, *Angew. Chem., Int. Ed.*, 2012, **51**, 1830–1834; (*b*) B. Kong, A. W. Zhu,

C. Q. Ding, X. M. Zhao, B. Li and Y. Tian, *Adv. Mater.*, 2012, **24**, 5844–5848; (*c*) A. W. Zhu, Q. Qu, X. L. Shao, B. Kong and Y. Tian, *Angew. Chem., Int. Ed.*, 2012, **51**, 7185–7189.
7 M. V. Ekharsky and Y. Inoue, *Chem. Rev.*, 1998, **98**, 1875–1918.
8 (*a*) A. Harada, *Acc. Chem. Res.*, 2001, **34**, 456–464; (*b*) A. Kulkarni, K. DeFrees, S. Hyun and D. H. Thompson, *J. Am. Chem. Soc.*, 2012, **134**, 7596–7599; (*c*) J. X. Zhang, H. L. Sun and P. X. Ma, *ACS Nano*, 2010, **4**, 1049–1059.
9 B. Balan, D. L. Sivadas and K. R. Gopidas, *Org. Lett.*, 2007, **9**, 2709–2712.
10 N. S. Makarov, M. Drobizhev and A. Rebane, *Opt. Express*, 2008, **16**, 4029–4047.
11 (*a*) F. Danhier, A. L. Breton and V. Préat, *Mol. Pharmaceutics*, 2012, **9**, 2961–2973; (*b*) M. Théry, V. Racine, A. Pepin, M. Piel, Y. Chen, J. B. Sibarita and M. Bornens, *Nat. Cell Biol.*, 2005, **7**, 947–953.
12 (*a*) M. Oba, K. Aoyagi, K. Miyata, Y. Matsumoto, K. Itaka, N. Nishiyama, Y. Yamasaki, H. Koyama and K. Kataoka, *Mol. Pharmaceutics*, 2008, **5**, 1080–1092; (*b*) M. Oba, S. Fukushima, N. Kanayama, K. Aoyagi, N. Nishiyama, H. Koyama and K. Kataoka, *Bioconjugate Chem.*, 2007, **18**, 1415–1423.